Applied Catalysis B: Environmental 224 (2018) 634–647

Contents lists available at ScienceDirect

Applied Catalysis B: Environmental

journal homepage: www.elsevier.com/locate/apcatb

Research paper

# Insight into pathways of methylene blue degradation with $H_2O_2$ over mono and bimetallic Nb, Zn oxides

Lukasz Wolski*, Maria Ziolek

*Adam Mickiewicz University in Poznan, Faculty of Chemistry, Umultowska 89b, 61-614 Poznan, Poland*

ARTICLE INFO

*Keywords:*
$Nb_2O_5$
$ZnNb_2O_6$
Surface properties
Interaction with $H_2O_2$
Methylene blue degradation

ABSTRACT

The aim of this work was to investigate the influence of surface properties of metal oxides ($Nb_2O_5$, ZnO and $ZnNb_2O_6$) on the type of reactive oxygen species (ROS) formed in contact with hydrogen peroxide, and to determine the effect of zinc addition to niobium pentoxide on the type of ROS formed and its activity in methylene blue degradation. The structure and surface properties of materials synthesized were characterized by nitrogen adsorption, XRD, XPS, SEM, SEM-EDX, DR UV–vis and FTIR techniques. The ability of metal oxides to generate superoxo and peroxo species upon treatment with $H_2O_2$ was documented and discussed in respect to the type of metal oxide used. It was found that the distortion of $NbO_6$ species in bimetallic oxide influenced the interaction of this mixed oxide with hydrogen peroxide. The oxidative properties of reactive oxygen species formed on the surface of metal oxides were tested in degradation of methylene blue. The activity of niobium(V) oxide in this process was much higher than that of mixed oxide and ZnO. In order to identify the reaction pathways on the basis of determination of the reaction intermediates, the reaction mixtures were analyzed by ESI–MS. On the basis of the results obtained the mechanism of the dye degradation was discussed.

## 1. Introduction

In recent years the oxidation processes with the use of environmentally benign oxidants (instead of chromates or permanganates) have attracted much attention because of their numerous advantages [1]. These oxidants include reactive oxygen species (ROS) such as hydroxyl radicals (HO·), peroxides ($O_2^{2-}$) and superoxide anions ($O_2\cdot^-$) formed by the decomposition of hydrogen peroxide ($H_2O_2$). According to literature [2–9] ROS can be generated *in situ* on the surface of selected metal oxides (e.g. $Nb_2O_5$, $V_2O_5$, $TiO_2$, $Fe_2O_3$) by the treatment with hydrogen peroxide, and then successfully used as heterogeneous catalysts for environmentally benign epoxidation of olefins [2,3,5,10], selective oxidation of alcohols [4,8] and degradation of organic pollutants [11–13]. This possibility illustrates a great potential of their application for environmentally friendly oxidation processes.

One of the most investigated metal oxides in terms of interaction with $H_2O_2$ that leads to formation of ROS is niobium pentoxide. It was documented that the treatment of this metal oxide with $H_2O_2$ leads to generation of strongly oxidative species such as $O_2\cdot^-$ and $O_2^{2-}$ [8]. Many authors have reported that combining niobium pentoxide with other metals may enhance its ability to formation of ROS, and thus may influence the catalytic activity of the composite. Oliveira et al. [14] have investigated the influence of iron oxide addition to niobia on its activity in degradation of organic dyes. It was found that iron:niobia composite (Fe:Nb = 1:1) exhibited remarkably higher degradation efficiency than mono metal oxides. The enhancement of catalytic activity of the system resulted from higher accessibility of surface species, which were active in decomposition of $H_2O_2$ into HO· and $HO_2\cdot$. Cardoso et al. [15] have investigated the effect of tungsten doping on catalytic properties of niobium pentoxide. The authors evidenced that modification of niobia with tungsten led to an increase in the efficiency of methylene blue degradation. The high catalytic activity of Nb:W composite in this reaction resulted from its enhanced ability to formation of strongly oxidizing peroxo species. Besides $Nb_2O_5$, another promising material in terms of interaction with hydrogen peroxide is ZnO. Treatment of this metal oxide with $H_2O_2$ leads to formation of zinc peroxide, which was found to be highly active in selective oxidation of aromatic alcohols [4]. Combining of niobium pentoxide and zinc oxide (well-known metal oxides) and formation of mixed niobium-zinc oxide would lead to obtaining material with interesting catalytic properties.

Mixed niobium–zinc oxide ($ZnNb_2O_6$) is known in literature because of its excellent dielectric properties that make this material an attractive candidate for microwave devices [16–18]. $ZnNb_2O_6$ is also a promising photocatalyst that can be successfully used for degradation of dyes [19,20], hazardous organic compounds [20] and for photocatalytic water splitting [21]. To the best of our knowledge, there are

* Corresponding author.
*E-mail address:* wolski.lukasz@amu.edu.pl (L. Wolski).

https://doi.org/10.1016/j.apcatb.2017.11.008
Received 28 June 2017; Received in revised form 13 October 2017; Accepted 4 November 2017
Available online 06 November 2017
0926-3373/ 

no reports regarding the interaction of hydrogen peroxide with mixed niobium-zinc oxides (e.g. $ZnNb_2O_6$), and generation of reactive oxygen species on its surface.

The aim of this study was to investigate the influence of surface properties of $Nb_2O_5$, ZnO and $ZnNb_2O_6$ on the type of reactive oxygen species that are formed on their surfaces upon treatment with hydrogen peroxide, and to determine the effect of zinc addition to niobium pentoxide on the ability to ROS formation and its activity in degradation of methylene blue. Moreover, the reaction pathways were tracked in order to determine the mechanism of methylene blue degradation.

## 2. Experimental

### 2.1. Synthesis of materials

#### 2.1.1. Reagents

Niobium(V) ethoxide ($Nb(OCH_2CH_3)_5$, Aldrich, 99.95%), zinc(II) acetate ($Zn(O_2CCH_3)_2$, Aldrich, anhydrous, 99.99%), surfactant Pluronic P123 (triblock copolymer poly(ethylene glycol)-block-poly (propylene glycol)-block-poly(ethylene glycol), Aldrich, M = 5800 g $mol^{-1}$), hydrochloric acid (POCH, 35%-38%, pure p.a.), acetic acid (POCH, 99.5%-99.9%), methanol (POCH, ≥99.98%), hydrogen peroxide (POCH, 30%), methylene blue (Aldrich, dye content ≥ 82%), o-phenylenediamine peroxidase substrate (OPD, Aldrich, ≥98.0%) were all used in analytical grade without further purification.

#### 2.1.2. Synthesis procedure

Niobium(V) oxide, zinc(II) oxide and mixed niobium-zinc oxide were prepared according to a modified Suzuki et al. procedure [22]. The amounts of reagents used during the synthesis of metal oxides are given in Table 1. For the synthesis of mixed niobium-zinc oxide, the equimolar amounts of niobium and zinc were used (Nb:Zn molar ratio = 1).

In a typical synthesis route, Pluronic P123 surfactant was dissolved in methanol. Next, concentrated hydrochloric acid and acetic acid were added. Following 30 min of stirring at room temperature (RT) the source of metal was added upon continuous stirring. For the synthesis of mixed niobium-zinc oxide, the zinc source ($Zn(O_2CCH_3)_2$) was firstly dissolved in methanol, and then added to the reaction mixture. That is why greater amount of methanol was used in the synthesis of mixed niobium-zinc oxide, than in the synthesis of niobium pentoxide and zinc (II) oxide. The sources of metal (Nb and Zn) were added in the following order: zinc containing solution, then niobium(V) ethoxide. After the metal source addition, the reaction mixture was stirred for 1 h at RT, then transferred into petri dishes in the form of thin layer, and dried for 12 h at 313 K and the next 24 h at 338 K. The gel obtained was calcined at 773 K for 5 h (temperature ramp: 2 K $min^{-1}$). The calcination temperature was chosen on the basis of results obtained by Suzuki et al. [22] who have reported that the calcination of $Nb_2O_5$ at 673 K led to obtaining of material with higher surface area than that calcined at 773 K (ca 200 $m^2$ $g^{-1}$ vs ca 50 $m^2$ $g^{-1}$), but definitely smaller pore size (ca 5 nm vs ca 16 nm). Because of the application of the catalyst prepared in this work to oxidation processes performed in liquid phase, and because of large size of dye molecule (methylene blue), the larger pore size was required. Therefore 773 K was chosen as calcination temperature to obtain materials with moderate surface area and large pore size. Calcination at 873 K was not considered due to collapse of porous structure under these conditions that resulted in very low surface area of materials obtained (~3 $m^2$ $g^{-1}$) [22]. The metal oxides prepared in this work were denoted as: $Nb_2O_5$, ZnO and $ZnNb_2O_6$.

### 2.2. Characterization of materials

Characterization of materials was performed by the standard methods allowing the characterization of structure/texture parameters of the prepared metal oxides (XRD, $N_2$ adsorption/desorption, SEM, EDX), whereas UV-vis, FTIR and XP spectroscopies were used for the characterization of surface species.

The XRD patterns were recorded on a D8 Advance diffractometer (Bruker) using CuKα radiation (λ = 0.154 nm), with a step size of 0.05° in the 2Θ = 6–60° range. The average crystallite size was calculated using the Scherrer equation.

The $N_2$ adsorption-desorption isotherms were obtained at 77 K using a Micromeritics ASAP 2020 Physisorption Analyzer. Before the measurements, the samples were degassed at 573 K for 8 h. The surface area of the materials obtained was calculated by the BET method, and the average pore size was estimated from the adsorption branch.

The morphology of the synthesized catalysts was investigated using a field-emission scanning electron microscope (FE-SEM) type JEOL JSM 7401F operating at the accelerating voltage of 5 kV. Energy Dispersive X-ray analysis (EDX) and EDX mapping were performed using the accelerating voltage of 15 kV and an EDAX Genesis XM2 Imaging System composed of a 10 $mm^2$ Si(Li) detector with SUTW window for detection of all elements down to Be, the digital electronics and software for image acquisition and X-ray signal mapping as well as qualitative and quantitative analysis capabilities.

Diffuse reflectance UV–vis spectra (DR UV–vis) were recorded on a Varian Cary 300 Scan spectrophotometer equipped with a diffuse reflectance accessory. The spectra were recorded at room temperature in the range from 200 to 800 nm. Spectralon was used as the reference material. The direct band gap of metal oxides was estimated using the Tauc plot method [23].

FTIR spectra of samples were acquired in the range from 4000 $cm^{-1}$ to 400 $cm^{-1}$ (resolution 4 $cm^{-1}$, number of scans = 64) using a Bruker Vertex 70 spectrophotometer. For the FTIR measurements with KBr, metal oxides were dispersed in KBr pellet (5 mg of the sample and 200 mg of KBr). FTIR − ATR (Attenuated Total Reflectance) spectra were recorded for the powdered samples (without KBr) using a Platinum ATR accessory (Bruker).

X-ray photoelectron spectroscopy (XPS) was performed using an ultra-high vacuum photoelectron spectrometer based on Phoibos150 NAP analyzer (Specs, Germany). The analysis chamber was operated under vacuum with a pressure close to $5 \times 10^{-9}$ mbar and the sample was irradiated with a monochromatic Al Kα (1486.6 eV) radiation. Any charging that occurred during the measurements (due to incomplete neutralization of ejected surface electrons) was accounted for by rigidly shifting the entire spectrum by a distance needed to set the binding energy of the C1s assigned to adventitious carbon to the assumed value of 284.8 eV.

**Table 1**
Reagents used for the synthesis of metal oxides.

| Metal oxide | Reagents | | | | | |
|---|---|---|---|---|---|---|
| | $Nb(OCH_2CH_3)_5$ [mmol] | $Zn(CH_3COO)_2$ [mmol] | Pluronic P123 [mmol] | HCl [mL] | $CH_3COOH$ [mL] | $CH_3OH$ |
| $Nb_2O_5$ | 84 | – | 4.61 | 8.9 | 19.2 | 252 |
| ZnO | – | 84 | 4.61 | 8.9 | 19.2 | 252 |
| $ZnNb_2O_6$ | 42 | 42 | 4.61 | 8.9 | 19.2 | 380 |

### 2.3. Treatment with hydrogen peroxide

In order to investigate the influence of zinc addition on the $Nb_2O_5$ ability to generate active oxygen species upon contact with hydrogen peroxide, the synthesized metal oxides were treated with this oxidant. The treatment was performed by dropwise addition of hydrogen peroxide (0.5 mL) to metal oxides (11 mg) at RT. Hydrogen peroxide was applied in excess to simulate the conditions of the oxidation reaction in which hydrogen peroxide is used as an oxidant and metal oxide as a catalyst.

The ability of this catalyst to generate hydroxyl radicals was investigated with the use of o-phenylenediamine peroxidase substrate (OPD). OPD selectively reacts with hydroxyl radicals leading to formation of 2,3-diaminophenazin, which absorbs light at ca 440 nm [24]. This allows tracking the formation of hydroxyl radicals by UV–vis spectroscopy. In a typical experiment, 80 mL of OPD solution in water (1.2 mmol $L^{-1}$) was added to 30 mg of catalyst. Next pH of the reaction mixture was adjusted to 5.2 with the use of nitric acid. After the pH adjustment 4.2 mL of hydrogen peroxide (30%) was added upon intensive stirring. The reaction was performed in a dark chamber at room temperature. After the proper time of reaction (30 and 60 min), 4 mL of aliquot was withdrawn from the mixture, and the catalyst was separated by filtration through a 0.2 µm Millipore filter. The absorbance of filtrate was measured in the range from 190 nm to 800 nm with the use of Varian, Cary 300 UV–vis spectrophotometer.

### 2.4. Test of catalytic activity

#### 2.4.1. Degradation of methylene blue

Oxidative properties of reactive oxygen species formed on the surface of metal oxides were evaluated by discoloration of methylene blue (MB) at room temperature. In a typical reaction, 0.1 g of catalyst was dispersed in 5 mL of hydrogen peroxide (30%). Next, 95 mL of MB solution (15 mg $L^{-1}$ or 37.5 mg $L^{-1}$) was added. In order to avoid photocatalytic degradation of methylene blue, the reactions were performed in the dark chamber. The dye discoloration was monitored using UV–vis spectroscopy (Varian, Cary 300 UV–vis spectrophotometer). For this purpose, after the proper time, 4 mL of the reaction mixture was removed, and the catalyst was separated from the solution by filtration through a 0.2 µm Millipore filter. The efficiency of methylene blue removal was calculated using the following equation (Eq. (1)):

$$Efficiency\ of\ MB\ discoloration = \frac{C_0 - C}{C_0} x100\% = \frac{A_0 - A}{A_0} x100\% \quad (1)$$

where $A_0$ is the absorbance of the initial MB solution, $C_0$ is the initial concentration of MB, A is the absorbance of the MB solution after a given time of the reaction, and C is the concentration of MB after a given time of the reaction; the absorbance was measured at 664 nm. For the sorption capacity measurements water was used instead of hydrogen peroxide. The pH of the reaction mixtures was adjusted using $HNO_3$.

#### 2.4.2. ESI–MS studies

Products of methylene blue degradation were identified with the use of QTOF mass spectrometer (Impact HD, Bruker) in positive ion mode. The reaction mixtures were diluted 100 times prior the analysis. The diluted reaction samples were injected into the ESI source with a syringe pump at a flow rate of 3 µL $min^{-1}$. The ESI conditions were as follows: heated capillary temperature of 473 K, sheath gas ($N_2$) at a flow rate of 4 L $min^{-1}$, capillary voltage of 3600 V.

## 3. Results and discussion

### 3.1. Characterization of metal oxides

#### 3.1.1. X-ray diffraction (XRD)

X-ray diffraction patterns recorded for the synthesized metal oxides are shown in Fig. 1. $Nb_2O_5$ and ZnO exhibited hexagonal structure that was fitted to JCPDS card No. 00-007-0061 and 01-089-1397, respectively. Mixed

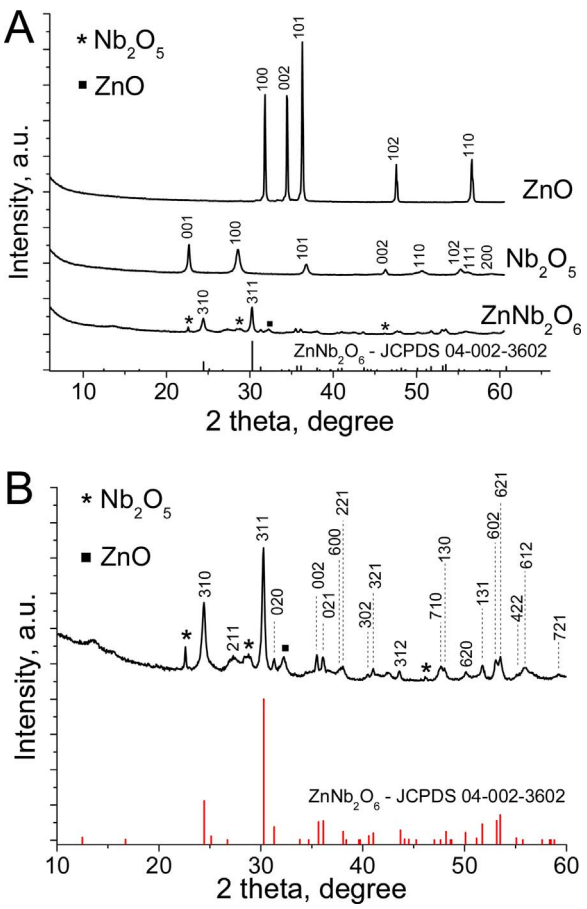


**Fig. 1.** XRD patterns of synthesized metal oxides (A) and comparison of XRD pattern of as-prepared mixed niobium-zinc oxide with orthorhombic crystal system of $ZnNb_2O_6$ (JCPDS card No. 04-002-3602) (B).

niobium-zinc oxide crystalized in orthorhombic crystal system of $ZnNb_2O_6$ (JCPDS card No. 04-002-3602), and the presence of this phase was confirmed by high intensity peaks at 2 theta degree equal to 24.4 and 30.3 which are characteristic of (310) and (311) planes of $ZnNb_2O_6$, respectively. XRD pattern of mixed niobium-zinc oxide revealed also the presence of three low intensity peaks typical of (001), (100) and (002) planes of $Nb_2O_5$ and one low intensity peak characteristic of (100) plane of ZnO. It indicates that not all niobium and zinc species participated in the formation of the mixed phase.

The average crystallite sizes calculated from X-ray diffraction patterns using the Scherrer equation are shown in Table 2. $Nb_2O_5$ and $ZnNb_2O_6$ exhibited comparable crystallite sizes, which were found to be 61 and 57 nm, respectively. In contrast, the crystallite size of ZnO was significantly bigger in comparison to those of $Nb_2O_5$ and $ZnNb_2O_6$, and was found to be 101 nm.

**Table 2**
BET surface area, average pore size, average crystallite size and direct band gap of synthesized materials.

| Metal oxide | BET surface area [$m^2 g^{-1}$] | Average pore size[a] [nm] | Average pore volume[a] [$cm^3 g^{-1}$] | Average crystallite size[b] [nm] | Direct band gap[c] [eV] |
|---|---|---|---|---|---|
| $Nb_2O_5$ | 46 | 12.8 | 0.15 | 61 | 3.40 |
| ZnO | < 1 | – | – | 101 | 3.17 |
| $ZnNb_2O_6$ | 38 | 18.4 | 0.19 | 57 | 3.95 |

[a] calculated from adsorption branch using BJH method.
[b] estimated using Scherrer equation from (001), (311), (101) planes of $Nb_2O_5$, $ZnNb_2O_6$ and ZnO, respectively.
[c] estimated using Tauc plot method.

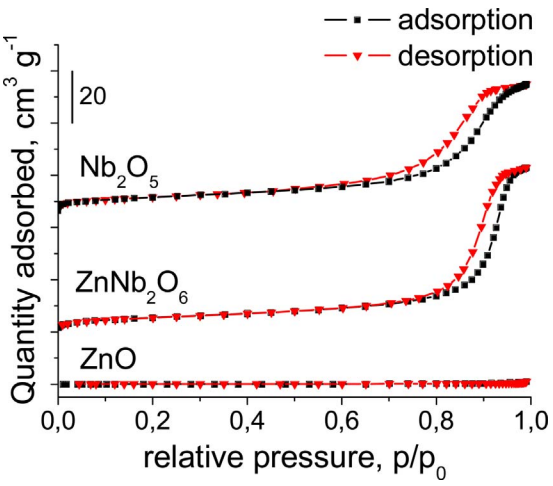


**Fig. 2.** Isotherms of nitrogen adsorption-desorption recorded for metal oxides.

### 3.1.2. BET surface area and pore size distribution

Nitrogen adsorption isotherms of niobium pentoxide and mixed niobium-zinc oxide (Fig. 2) were of type IV (according to UPAC classification) with a hysteresis loop typical of mesoporous materials. In contrast, the nitrogen adsorption isotherm of zinc oxide was typical of nonporous materials. The lack of porous structure of ZnO can be explained by the instability of mesostructure of zinc oxide during thermal treatment at high temperature which was performed for template removal [25]. BET surface areas and average pore sizes of prepared materials calculated from $N_2$ adsorption-desorption measurements are shown in Table 2. The lowest surface area ($< 1\ m^2\ g^{-1}$) was found for ZnO. Surface areas of $Nb_2O_5$ and $ZnNb_2O_6$ were significantly larger, of 46 and $38\ m^2\ g^{-1}$, respectively. Average pore size determined for mixed niobium-zinc oxide was 18.4 nm, and was larger than for niobium pentoxide (12.8 nm).

### 3.1.3. SEM-EDX

Different morphologies of all prepared samples were concluded from SEM images shown in Fig. 3. Both, $Nb_2O_5$ (Fig. 3A') and $ZnNb_2O_6$ (Fig. 3B') consisted of particles fused into the porous structure, while ZnO (Fig. 3C') contained larger, mainly nonporous particles of different shapes and sizes. Fig. 3B and B' show the particles of mixed niobium-zinc oxide which were mainly sphere-like with a small fraction of rod-like particles, and their sizes varied in the range from 30 to 125 nm (Fig. S1–SD) with average size of 69.8 nm. It is in agreement with the size of particles estimated from XRD patterns.

The distribution of niobium and zinc in mixed niobium-zinc oxide was investigated using SEM-EDX. The results obtained are shown in

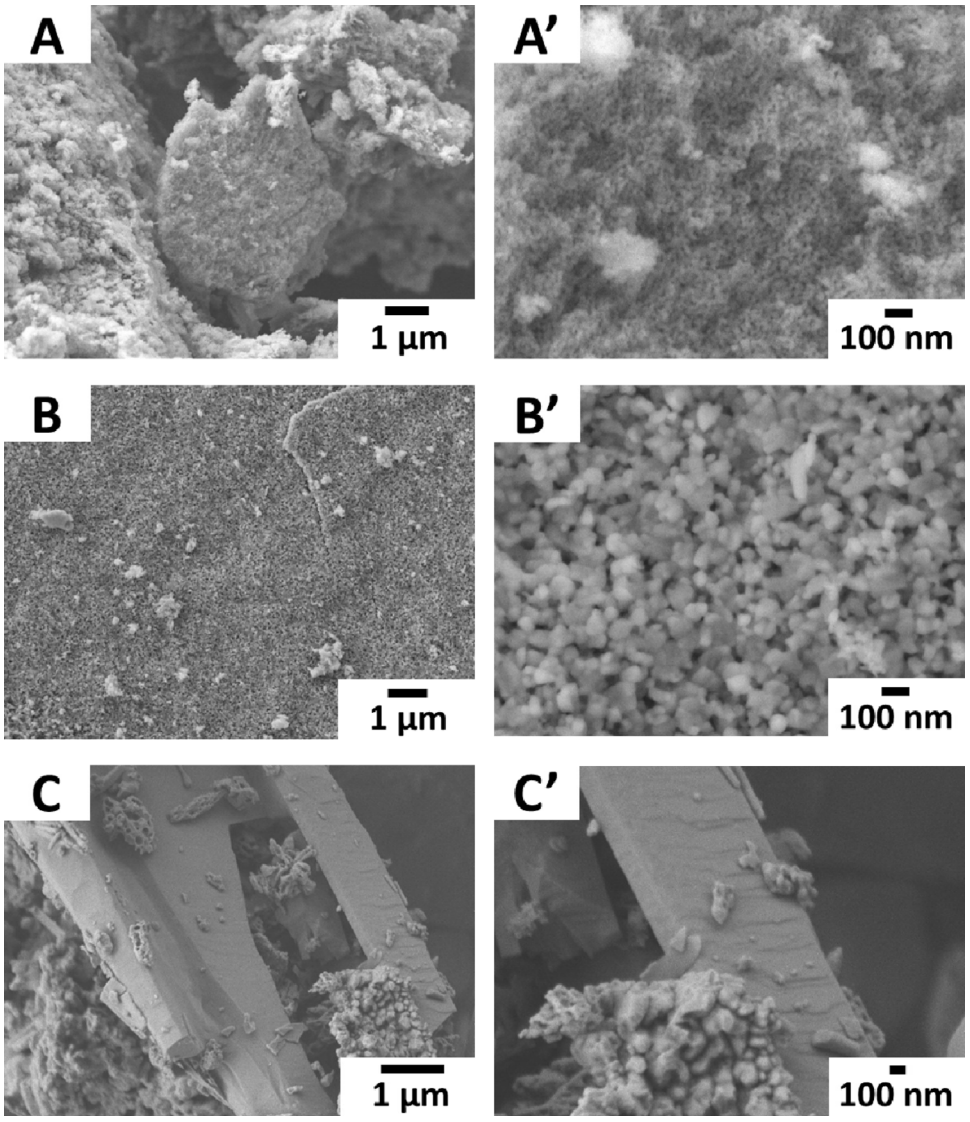


**Fig. 3.** SEM images of $Nb_2O_5$ (A, A'), $ZnNb_2O_6$ (B, B') and ZnO (C, C') at different magnification.

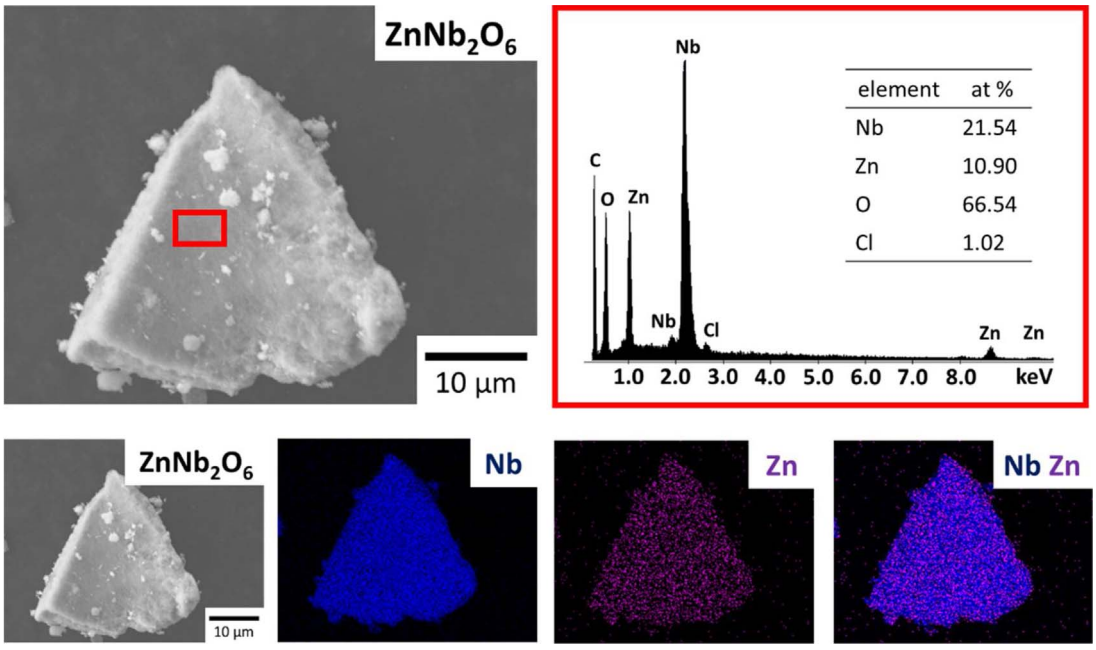


**Fig. 4.** SEM-EDX analysis and EDX mapping of mixed niobium-zinc oxide.

Fig. 4 and Fig. S2–SD. It is clear that niobium and zinc were homogenously distributed in the mixed oxide and the Nb:Zn atomic ratio was equal to 1.97 (Fig. 4). However, one can find the regions with inhomogeneous distribution of both metals, far from this atomic ratio, i.e. the regions with a higher concentration of niobium or zinc (Fig. S3–SD). EDX analysis performed for these regions revealed that Nb:Zn atomic ratio was either higher or lower than 2, namely 2.44 or 1.72, respectively. Literature data shows that the presence of nonstoichiometric compositions of columbite niobates ($M^{2+}Nb_2O_6$, where M = metal) with slight excess of either niobium or other metal instead of stoichiometric $M^{2+}Nb_2O_6$ is possible and may result from the instability of the nominal composition [26–28]. EDS analysis performed for $MnNb_2O_6$ by Gracia-Alvarado et al. [28] revealed that this material consisted of two types of particles: larger ones, which had excess of niobium (Nb:Mn ratio = 2.37), and smaller ones, which exhibited excess of zinc (Nb:Mn ratio = 1.80). The authors found that such variations of composition were not large enough to be detected by XRD analysis, and XRD patterns recorded for this material revealed the presence of single phase characteristic of $MnNb_2O_6$ (any additional peak was found). On the basis of results obtained the authors stated that this mixed metal oxide consisted of two nonstoichiometric oxides ($Mn_{0.9}Nb_{2.1}O_6$ and $Mn_{1.1}Nb_{1.9}O_6$), which were in the ratio of 80/20 to ensure average (stoichiometric) composition of $MnNb_2O_6$. In our work, XRD patterns clearly indicated the presence of additional phases (besides $ZnNb_2O_6$) characteristic of niobium pentoxide and zinc oxide. Furthermore, Nb:Zn atomic ratio higher or lower than two was observed only for regions where additional phase was observed in the images (Fig. S3–SD). These observations led us to conclude that Nb:Zn atomic ratio far from 2 is more likely due to the presence of bulk niobium and zinc oxides on the surface of $ZnNb_2O_6$, than the presence of nonstoichiometric mixed niobium-zinc oxide. It is important to emphasis that the regions with an excess of niobium or zinc were in minority, and were presented only for precisely characterization of the materials prepared. Regions where Nb:Zn atomic ratio was of 2 predominated and were assigned to stoichiometric $ZnNb_2O_6$.

### 3.1.4. Infrared spectroscopy

FTIR spectra of metal oxides in KBr tablets are shown in Fig. 5. The most intensive bands in the absorption spectrum of $Nb_2O_5$ were at around 880 and 616 $cm^{-1}$. According to literature, the first one is attributed to vibrations of isolated $NbO_x$ surface species with long Nb═O bonds [29], or to the stretching modes of Nb−O−Nb bonds in polymerized $NbO_x$ species [30]. The band at 616 $cm^{-1}$ is assigned to the symmetric stretching of Nb−O bonds [31]. The less intense band observed in FTIR spectrum at around 818 $cm^{-1}$ is also characteristic of $Nb_2O_5$ and is attributed to the asymmetric stretching of $[-O-Nb-O]_n$ bonds [31]. The spectrum recorded for zinc oxide revealed one intense band at 495 $cm^{-1}$, and three low intensity bands at 728, 1047 and 1159 $cm^{-1}$. The first band at 495 $cm^{-1}$ is related to the vibration modes characteristic of ZnO phase [32]. The bands at about 728, 1047 and 1159 $cm^{-1}$ are related to the presence of C═O, C−OH and C−O vibrational modes, respectively and indicate the presence of organic residual from the template. It was found that for $ZnNb_2O_6$ the vibration band at ca 880 $cm^{-1}$ which is characteristic of isolated $NbO_x$ surface species with long Nb═O bonds [29] was not observed. However, the spectrum recorded for this mixed metal oxide contained two other vibrational bands at ca 980, 953 $cm^{-1}$, which were not observed for $Nb_2O_5$. According to literature, the first new band at 980 $cm^{-1}$ is attributed to the same type of niobium species as observed at 880 $cm^{-1}$ (i.e. Nb═O), but with a shorter Nb═O bond length [29]. The second band at ca 953 $cm^{-1}$ observed in FTIR spectrum of $ZnNb_2O_6$ is related to the presence of niobium species with moderate Nb═O bond length (longer than for the species characterized by the band at 980 $cm^{-1}$ but shorter than for the species observed at 880 $cm^{-1}$) [29].

### 3.1.5. Optical properties (UV–vis results)

Optical properties of metal oxides were investigated by diffuse reflectance UV–vis spectroscopy. The band gap values of the materials were estimated from UV–vis spectra using the Tauc plot method. The results obtained are presented in Table 2 and Fig. S4–SD. The smallest band gap value of 3.17 eV was obtained for ZnO. The band gap value of $Nb_2O_5$ was slightly higher (3.40 eV) than for ZnO, and the highest band gap was characteristic of $ZnNb_2O_6$ (3.95 eV). The estimated values of band gaps are in good agreement with previous reports regarding the optical properties of $Nb_2O_5$ [33], ZnO [33] and $ZnNb_2O_6$ [19,20], and confirmed the successful formation of $ZnNb_2O_6$ phase.

### 3.1.6. X-ray photoelectron spectroscopy (XPS)

XP spectra of O1s shown in Fig. 6 give information about the state of oxygen in mono- and bimetallic oxides. The shape of the spectra of

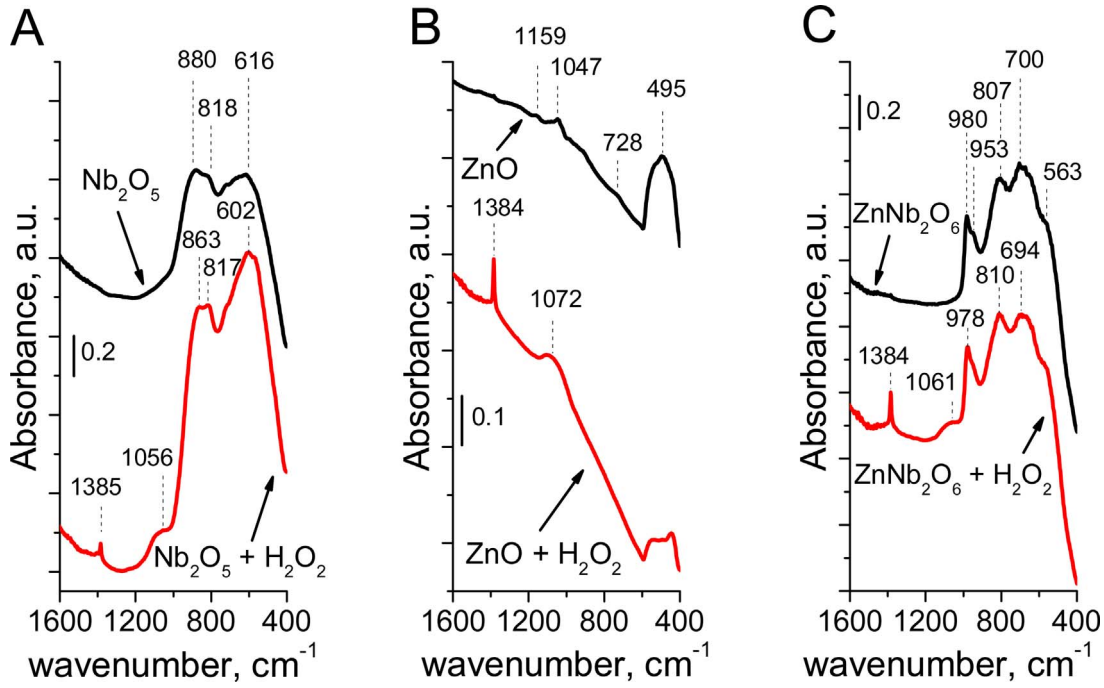


**Fig. 5.** FTIR spectra with KBr of $Nb_2O_5$ (A), ZnO (B), and $ZnNb_2O_6$ (C) before and after treatment with $H_2O_2$.

mono-metallic oxides strongly depends on the nature of metal. The XP spectrum of niobium oxide revealed one very intense band at BE ~530 eV with a small shoulder at a higher binding energy, whereas the spectrum of ZnO presented the same component at ca 530 eV but with a much higher shoulder at higher BE. The deconvolution of XP spectra allowed a detailed estimation of the bands positions and the distribution of both oxygen species (Table 3). According to literature [32,34] the XPS band in the region between 530.1 eV and 530.6 eV is due to the oxygen bonded to metal in metal oxide ($O^{2-}$ species), whereas the component at a higher BE (531.8–532 eV) is characteristic of M-OH species ($OH^-$). Interestingly, the contribution of the last component was less than 20% in $Nb_2O_5$, whereas in ZnO its contribution was ca 48%. High contribution of component at 531.8–532.0 eV observed for zinc oxide resulted from the presence of oxygen defects as was stated in [35]. It is important to stress that the region characteristic of M-OH species is overlapped with that characteristic of peroxide species [4,36,37]. Since the metal oxides were not treated with hydrogen peroxide during the synthesis, the component at 531.8–532 eV has to be related to surface hydroxyl groups or oxygen deficient regions. The traces of superoxo species were detected in $Nb_2O_5$ and $ZnNb_2O_6$. They can be formed during the calcination of oxides containing niobium in the presence of the template.

The shape of the $ZnNb_2O_6$ O1s spectrum is similar to that of niobium oxide. The difference is in the appearance of small amount (2.0%) of nucleophilic oxygen characteristic of cation-deficient regions. Such defects are important species for possible application of $ZnNb_2O_6$ as catalyst.

### 3.2. Characterization of metal oxides after treatment with $H_2O_2$

Metal oxides are often used in the catalytic oxidation of organic compounds with hydrogen peroxide. The crucial role in these processes plays the chemisorption of $H_2O_2$ leading to the formation of peroxo or superoxo species active in the oxidation of e.g. olefins or glycerol, respectively [8]. Metal peroxides and superoxides can be identified by infrared spectroscopy and UV–vis measurements. The results obtained by these two methods after the treatment of metal oxides with hydrogen peroxide are discussed below.

#### 3.2.1. UV–vis spectra and XRD study

The changes in optical properties of metal oxides after treatment with $H_2O_2$ were investigated with UV–vis spectroscopy. Fig. 7 reveals that the interaction of $H_2O_2$ with metal oxides entailed changes in their optical properties. The treatment of $Nb_2O_5$ with hydrogen peroxide resulted in the increase in the intensity of the band at 325 nm and the appearance of a new UV–vis band at 375 nm (separated after deconvolution), which are attributed to the ligand-to-metal charge transfer (LMCT) in superoxo and peroxo niobium species, respectively [38,39]. The interaction of $ZnNb_2O_6$ with $H_2O_2$ led to an increase in absorption at ca 339 nm, which is attributed to the formation of superoxo species. The shift of this band to higher wavelengths in comparison to its position in the spectrum of $Nb_2O_5$ results from different electronic properties of mixed niobium-zinc oxide. The fact of formation of peroxo species on $Nb_2O_5$ was confirmed by its yellow color after treatment with $H_2O_2$ (color comes from peroxo species), while no change in color after the same treatment was noted for $ZnNb_2O_6$. In the spectrum of ZnO sample no new band appeared upon the treatment with $H_2O_2$. However, as shown in Fig. 7 the interaction of ZnO with $H_2O_2$ led to a significant increase in the 270 nm band intensity. According to literature, the UV–vis band in this range of wavelengths can be attributed to the charge transfer in small ZnO nanoparticles [40–42] or in zinc peroxide [37]. As a decrease in the particle size upon $H_2O_2$ treatment is not expected, thus this phenomenon is more likely due to the formation of $ZnO_2$ on the surface of ZnO. H. Bai and X. Liu [43] have revealed that the treatment of ZnO with $H_2O_2$ at 50 °C may lead to the formation of a mixture of ZnO and $ZnO_2$. Treatment of ZnO with hydrogen peroxide at RT in this work led to the transformation of a significant amount of ZnO to $ZnO_2$ as evidenced from XRD patterns shown in Fig. S5–SD. The new peaks at 2Θ of 31.81, 36.87, 41.23, 45.51 and 53.06° are characteristic of $ZnO_2$ (JCPDS card No. 13-0351, [37]; peaks of ZnO before treatment with $H_2O_2$ were found at 2Θ equal to 31.74, 34.40, 36.23, 47.50, 56.57°). The generation of zinc peroxide is confirmed by the increase in areas ratio of the UV–vis bands at 270 nm and 337 nm before and after $H_2O_2$ treatment (Table S1–SD). The deconvolution of UV–vis spectrum recorded for ZnO revealed also that despite the increased area of the band at 270 nm, the treatment with $H_2O_2$ resulted in a slight increase in the ratio of areas of the bands at 270 nm and 370 nm (Table S1–SD). An increase in the intensity of the band at 370 nm could be also concluded

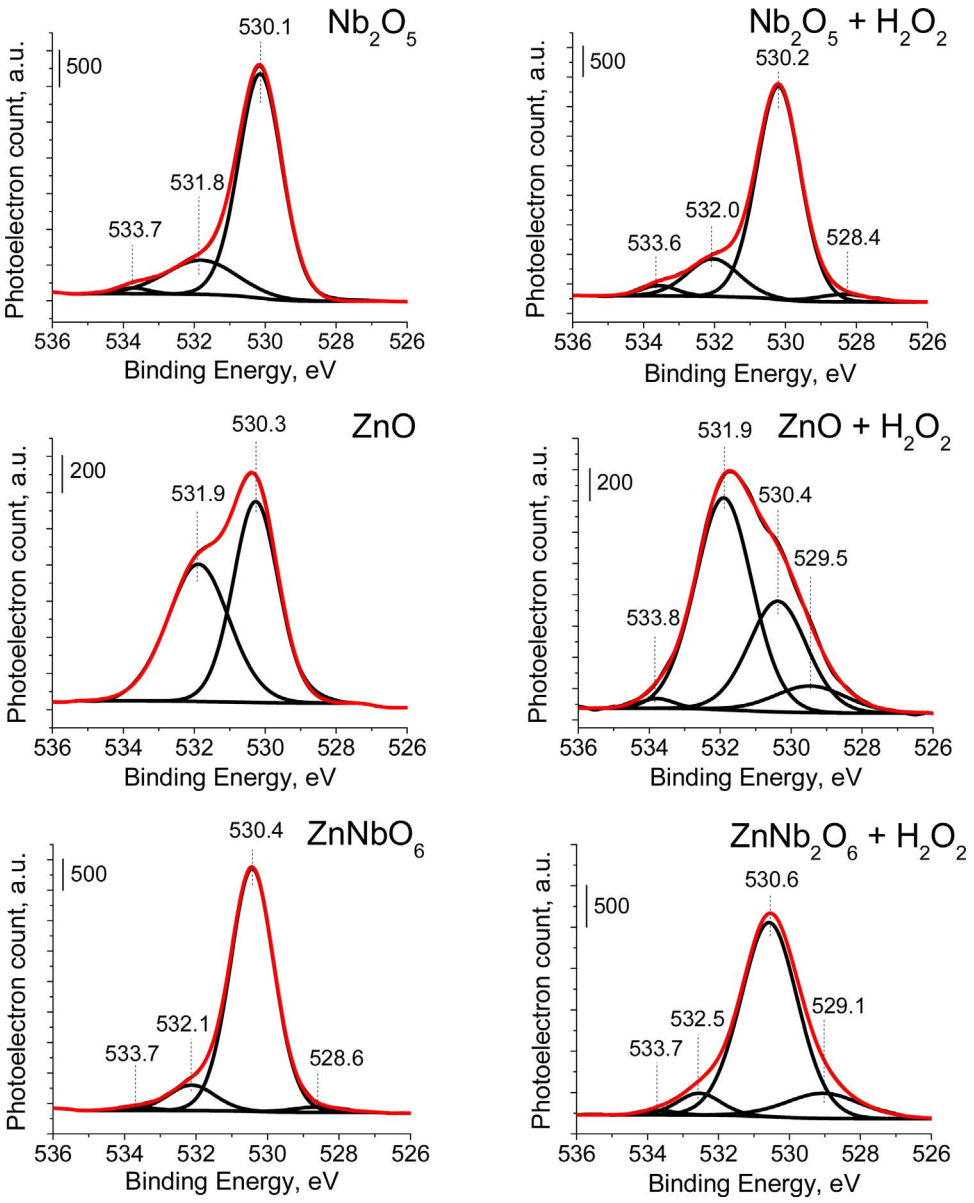


**Fig. 6.** XP spectra of O1s for parent oxides and the samples treated with hydrogen peroxide.

from Fig. 7. Such an increase in absorption of light at ca 370 nm indicates the formation of superoxo species on ZnO surface [38]. Another change in the optical properties of zinc oxide after hydrogen peroxide treatment is a decrease in the intensity of UV–vis band at about 335 nm caused by changes in the structure of ZnO. The explanation of this phenomenon is difficult on the basis of UV–vis measurement and thus it will be discussed in more detail in the next paragraph on FTIR measurements.

The ability of formation of hydroxyl radicals, another type of ROS, was estimated by the use of probe molecule, o-phenylenediamine (OPD). ODP solution with the catalyst was treated with hydrogen peroxide and the filtered solutions were analyzed by UV–vis spectroscopy

**Table 3**
Binding energies (O1s) and content of differen oxygen species in the parent materials and the samples treated with hydrogen peroxide.

| Metal oxide | Oxygen with the highest negative charge (nucleophilic species) | | Metal – oxide species | | M-OH/peroxo species | | Superoxo species | | Surface concentration of elements[a] [at %] | | |
|---|---|---|---|---|---|---|---|---|---|---|---|
| | BE [eV] | % | BE [eV] | % | BE [eV] | % | BE [eV] | % | Nb | Zn | O |
| $Nb_2O_5$ | – | – | 530.1 | 78.9 | 531.8 | 19.7 | 533.7 | 1.4 | 38.9 | – | 61.1 |
| $Nb_2O_5 + H_2O_2$ | 528.4 | 3.2 | 530.2 | 77.6 | 532.0 | 16.1 | 533.6 | 3.1 | 38.2 | – | 61.8 |
| ZnO | – | – | 530.3 | 51.9 | 531.9 | 48.1 | – | – | – | 52.1 | 47.9 |
| $ZnO + H_2O_2$ | 529.5 | 9.2 | 530.4 | 31.1 | 531.9 | 58.1 | 533.8 | 1.6 | – | 43.5 | 56.5 |
| $ZnNb_2O_6$ | 528.6 | 2.0 | 530.4 | 87.2 | 532.1 | 9.8 | 533.7 | 1.0 | 30.6 | 15.8 | 53.6 |
| $ZnNb_2O_6 + H_2O_2$ | 529.1 | 14.0 | 530.6 | 78.2 | 532.5 | 6.7 | 533.7 | 1.1 | 30.6 | 14.5 | 54.8 |

M – metal; BE – binding energy; % – content of oxygen species.
[a] calculated from XP spectra using CasaXPS software.

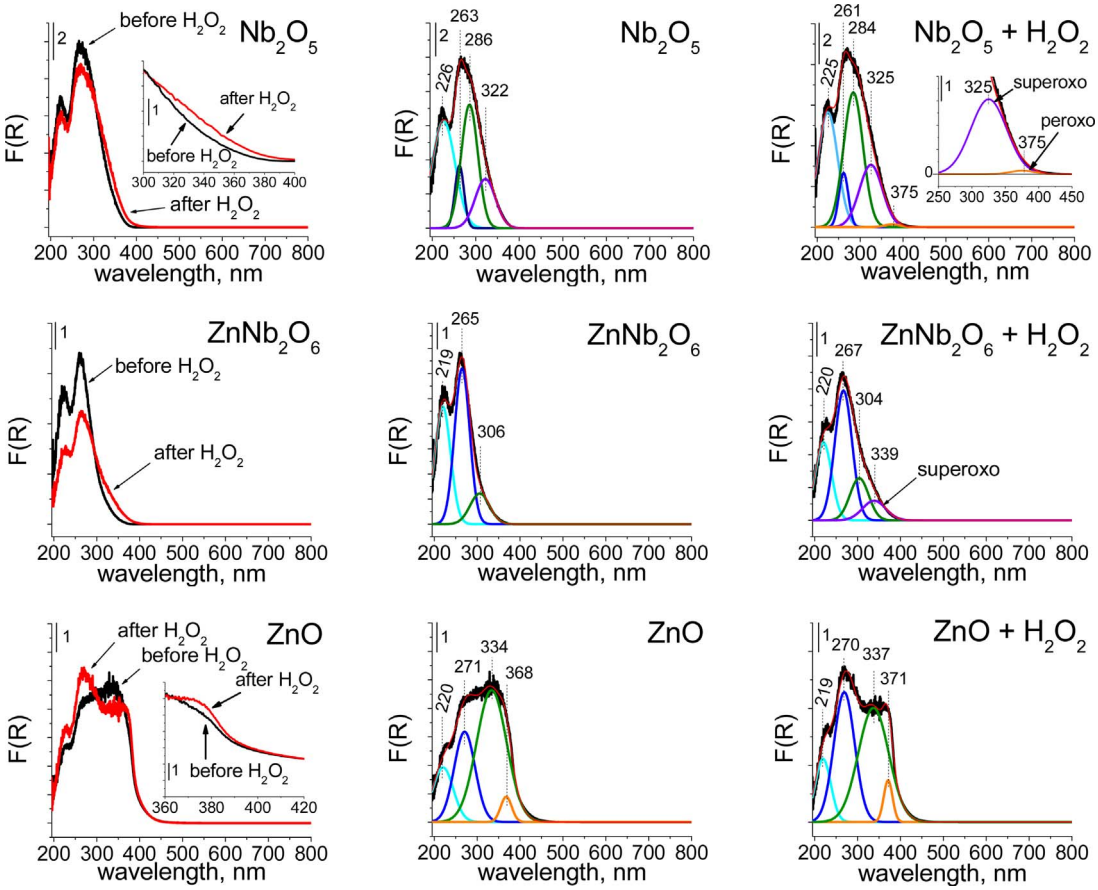


**Fig. 7.** Comparison of UV–vis DR spectra of samples recorded before and after the treatment with hydrogen peroxide (left side), and deconvolution of spectra before (middle row) and after treatment with $H_2O_2$ (right side).

after 30 and 60 min of the reaction. The results obtained shown in Fig. S6–SD indicated that without the catalyst only traces of 2,3-diaminophenazin (the product of OPD interaction with hydroxyl radicals) were detected in the relevant UV–vis spectrum (the band at ca 448 nm). When zinc oxide was added to the reaction mixture, the formation of HO· radicals was noticeable but the intensity of UV–vis band was only slightly higher than that obtained without the catalyst. The use of $ZnNb_2O_6$ caused a significant increase in the intensity of the band characteristic of 2,3-diaminophenazin, indicating very high ability of this catalysts to stimulate formation of hydroxyl radicals.

### 3.2.2. FTIR study

The FTIR spectra of metal oxides before and after $H_2O_2$ treatment are shown in Fig. 5. The treatment with $H_2O_2$ led to the appearance of a new broad band in the range from 1030 to 1150 $cm^{-1}$ irrespective of the type of oxides. It indicates generation of superoxo species on the surface of metal oxides [44]. The presence of hydrogen peroxide on the surface of metal oxides was indicated by the band at ca 1380 $cm^{-1}$ (Fig. 5) that is characteristic of vibrations modes in $H_2O_2$ molecules [45]. Fig. 5 shows the infrared bands at 1072, 1080 and 1078 $cm^{-1}$ in the spectra of ZnO, $ZnNb_2O_6$ and $Nb_2O_5$, respectively. These positions of IR bands are different than that of the band assigned to the vibrations in hydrogen peroxide. The above mentioned bands originate from the vibrations in metal superoxo species [44]. It is in a good agreement with the results of UV–vis measurements, and for ZnO confirms that a slight increase in the intensity of UV–vis band at ca 370 nm is related to the formation of superoxo species.

The FTIR spectra of niobium(V) oxide (Fig. 5A) showed changes in the positions of IR bands coming from Nb═O and Nb-O vibrations modes from 880 $cm^{-1}$ and 616 $cm^{-1}$ for $Nb_2O_5$ to 863 $cm^{-1}$ and 602 $cm^{-1}$ for the sample treated with $H_2O_2$. Such changes indicate the interaction of hydrogen peroxide with both niobium − oxygen species (formation of $NbO_7$ geometry; the Nb═O double bond becomes longer and also the lengths of the three axial Nb−O bonds are affected) [39]. The formation of peroxo species on the surface of niobium pentoxide was confirmed by FTIR-ATR measurement. As can be seen form Fig. 8A, the treatment with $H_2O_2$ led to the appearance of a broad band at about 865 $cm^{-1}$, which can be assigned to the stretching vibrations $\nu$(O−O) (peroxo) [8,46] formed on $Nb_2O_5$. This band can also results from a shift of an inflection at a lower wavelength present in the spectrum before $H_2O_2$ treatment, but there is no doubt that the intensity of the band (at 865 $cm^{-1}$) is much higher and therefore the assignment of this band to the vibration in new peroxo species is highly probable. Fig. 8B shows for $ZnNb_2O_6$ the inflection at ~875 $cm^{-1}$ before and after the treatment with $H_2O_2$. Thus, the FTIR-ATR spectra did not indicate changes on the surface of $ZnNb_2O_6$ after treatment with hydrogen peroxide. On ZnO material (Fig. 8C) no well-visible changes after $H_2O_2$ treatment are observed. It confirms the UV–vis results that revealed the formation of surface peroxo species only on $Nb_2O_5$. Fig. 5C shows also that for $ZnNb_2O_6$ no decrease in the intensity of the bands related to the $[-O-Nb-O-]_n$ vibrations modes was observed, which confirms that the nature of interaction of mixed niobium-zinc oxide with $H_2O_2$ is different than that of $Nb_2O_5$. Such differences in interaction of $Nb_2O_5$ and $ZnNb_2O_6$ with hydrogen peroxide resulted from different surface properties of these metal oxides (i.e. different Nb═O bond length). It is known that in niobium pentoxide, Nb═O species participate in formation of surface peroxo species [39,47]. In the case of $Nb_2O_5$, Nb═O bond length was longer than for $ZnNb_2O_6$ (as indicated by FTIR). It showed that shortening of Nb═O bond length may inhibit formation of peroxo species on the surface of niobium pentoxide. As can be seen

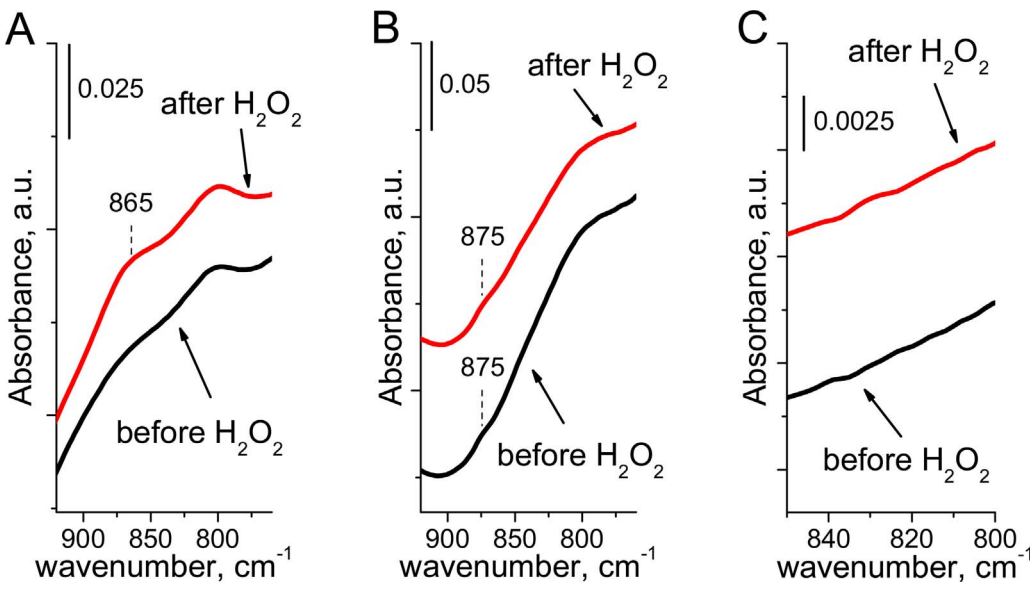


**Fig. 8.** FTIR – ATR spectra of $Nb_2O_5$ (A), $ZnNb_2O_6$ (B), and ZnO (C) before and after treatment with $H_2O_2$.

from Fig. 5B the treatment with $H_2O_2$ resulted also in changes in the FTIR spectrum of ZnO. It was found that after $H_2O_2$ addition the intensity of the band characteristic of zinc oxide structure, i.e. at 495 $cm^{-1}$, significantly decreased. The changes in the FTIR spectrum of zinc oxide indicate that the changes observed in optical properties of ZnO are not accidental. The decrease in intensity of the bands characteristic of ZnO structure may result from the formation of zinc peroxide.

### 3.2.3. X-ray photoelectron spectroscopy (XPS)

The changes in metal oxides caused by interaction with hydrogen peroxide can be tracked by XP spectroscopy. Fig. 6 shows the changes in XP spectra after treatment of the samples with hydrogen peroxide, whereas Table 3 indicates the values of BE for different oxygen species. In all XP spectra a characteristic broadening of the fundamental XPS band is observed after the interaction with hydrogen peroxide. The deconvolution of the spectrum of $Nb_2O_5$ treated with $H_2O_2$ indicated an increase in the area of the band characteristic of superoxo species and the formation of cation-deficient regions characterized by a band at 528.4 eV typical of oxygen with the excess of negative charge (strongly nucleophilic species). The much higher concentration of cation-deficient regions characterized by O1s band at 529.1 eV was observed in mixed niobium-zinc oxide treated with hydrogen peroxide (14% of oxygen total content). This observation suggests that hydrogen peroxide stimulated formation of the regions with the excess of oxygen ions. This process is more pronounced in $ZnNb_2O_6$ because of weaker interaction between niobium and oxygen caused by the deformation of $NbO_6$ octahedrons due to the interaction between niobium and zinc in the structure of $ZnNb_2O_6$. The significant shift in BE from 532.1 eV for parent $ZnNb_2O_6$ to 532.5 eV for mixed oxide treated with $H_2O_2$ has to be correlated with the formation of hydrogen-superoxo species. The latter resulted from the reaction $H_2O_2 + OH^- = HO_2^- + H_2O$ proposed in [8]. Hydrogen-superoxo species have a lower O1s BE than that of metal-superoxo species (BE at 533.7 eV). Traces of metal-superoxo species were also detected on bimetallic oxide before and after the treatment with $H_2O_2$. In zinc oxide treated with hydrogen peroxide the regions with excess of oxygen ions (BE O1s 529.5 eV) and metal superoxo species (BE O1s 533.8 eV) were detected. The increase in the area of the band at BE O1s 531.9 eV from 48.1% of the sum of areas of the bands characteristic of all oxygen species to 58.1% indicates the formation of metal-peroxo species documented by FTIR and UV–vis measurements.

### 3.3. Catalytic activity

Oxidative properties of ROS formed on the surface of metal oxides as a result of interaction with hydrogen peroxide were tested in discoloration of methylene blue as a model compound. The efficiency of discoloration process was monitored using UV–vis spectroscopy. It was a result of two processes, adsorption (measured by experiments in water solution) and catalytic oxidation/degradation. Fig. 9A illustrates the activity of materials during the experiment without pH adjustment. The highest activity and sorption capacity was characteristic of $Nb_2O_5$ (pH = 5.2). This catalyst removed 97% of methylene blue after 1 h of the reaction. Significantly lower sorption capacity and catalytic activity was characteristic of $ZnNb_2O_6$ (pH = 6.5; 64% of MB conversion after 5 h of reaction), while ZnO (pH = 6.7) was almost inactive in

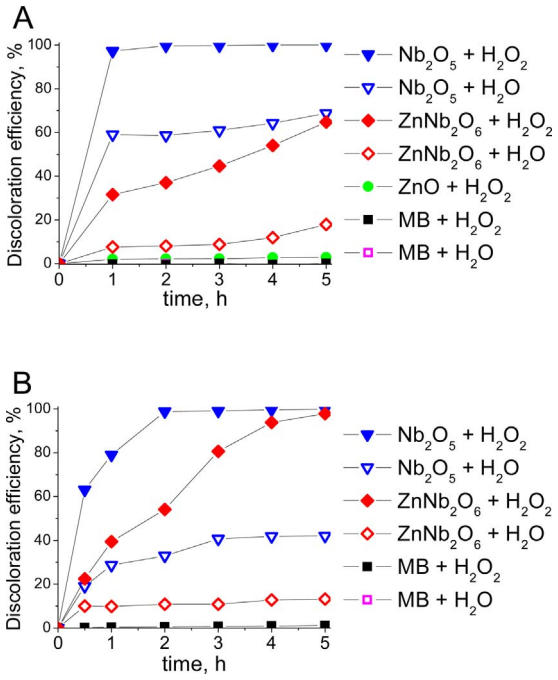


**Fig. 9.** The efficiency of MB discoloration process over metal oxides expressed by the percent of MB removal (discoloration efficiency) with the use different dye concentration and pH of reaction mixtures: A – MB concentration: 15 mg $L^{-1}$, no pH adjustment; B – MB concentration: 37.5 mg $L^{-1}$, pH adjusted to 5.0.

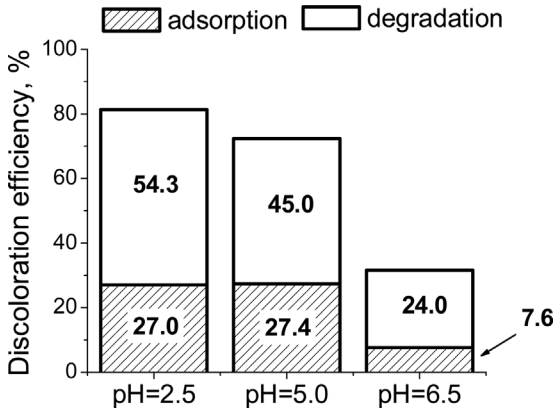


**Fig. 10.** The influence of pH of the reaction mixture on discoloration of MB over $ZnNb_2O_6$; dye concentration: 15 mg $L^{-1}$. Results after 1 h of reaction.

discoloration of methylene blue (2.8% of MB conversion after 5 h of reaction). Many authors have reported that the activity of materials in dye degradation processes is affected by pH of the reaction mixture [11,12]. In order to investigate if the difference in activity of $Nb_2O_5$ and $ZnNb_2O_6$ resulted from different pH of reaction mixtures, the experiment with pH adjustment was performed. Fig. 10 presents sorption capacity and catalytic activity of $ZnNb_2O_6$ in discoloration of the dye at different pH values. The decrease in pH of the reaction mixture resulted in enhancement of $ZnNb_2O_6$ sorption capacity from 7.6% at pH = 6.5 to 27.4% and 27.0% at pH = 5.0 and 2.5, respectively. The value of pH influences both, the charge on metal oxide surface and charge of MB. At a lower pH a positive charge of MB decreases [48,49] and raising the charge of the catalyst surface to that of MB molecules becomes beneficial for adsorption. It can be one of the reasons for the enhancement of sorption capacity. The efficiency of discoloration process was also related to the pH of reaction mixture. The lower the pH of reaction mixture, the higher the catalytic activity of material was observed. It is important to stress that for the reaction at pH = 2.5 and 5.0 the sorption capacities of mixed metal oxide were as comparable, while the MB conversion was higher at pH = 2.5 (54.3% vs 45.0%). However, even at lower pH the discoloration of MB did not achieve such a high value as on $Nb_2O_5$ (Fig. 9A).

In order to ensure that discoloration of methylene blue solution is effective also at higher concentration of the dye, another experiment with the use of 2.5 larger amount of methylene blue was performed (MB concentration = 37.5 mg $L^{-1}$) (Fig. 9B). Similarly to the reaction with lower concentration of the dye, $Nb_2O_5$ exhibited larger sorption capacity and catalytic activity than $ZnNb_2O_6$. After 1 h of the reaction in the presence of $Nb_2O_5$ the efficiency of discoloration process was almost twice higher than for $ZnNb_2O_6$ (78.9% vs 39.4%, Fig. 9B). It is important to stress that $Nb_2O_5$ converted almost 100% of MB after 2 h of the reaction, while for $ZnNb_2O_6$ discoloration process was much slower (97.8% of MB conversion after 5 h of the reaction). To compare the activity of $Nb_2O_5$ and $ZnNb_2O_6$, the kinetic constants of dye degradation at the initial step of reaction were calculated. In these conditions the reaction is expected to follow the first-order kinetics. The kinetic constants were determined by drawing a tangent at time t = 182 s on the concentration versus time profile. The results obtained are shown in Fig. S7–SD. Due to different catalysts ability to adsorb MB molecules, the efficiency of dye adsorption was taken into account in the calculation performed. It was found that the kinetic constant of MB degradation was significantly higher for $Nb_2O_5$ than for $ZnNb_2O_6$ ($24.57*10^{-7}$ $s^{-1}$ vs $5.92*10^{-7}$ $s^{-1}$).

Monitoring of the discoloration process using UV–vis did not give information about the mechanism of catalytic degradation and intermediates formed during this process. In order to estimate the reaction pathway the reaction mixtures were analyzed by ESI–MS. Literature data [11,12,14,50–54], in which ESI–MS was applied, indicated that MB degradation was initiated by the attack of hydroxyl radicals and the formation of hydroxylated compound ($m/z$ = 300) followed by the substitution of subsequent hydroxyl groups. After such hydroxylation the MB ring became broken and less complex organic compounds were formed. Some authors [55,56] have proposed a different reaction pathway via the formation of sulfoxide ($m/z$ = 303) which resulted from the interaction of MB with the catalyst surface. MB-sulfoxide was attacked by hydroxyl radicals towards degradation of methylene blue. In our work two parallel reaction pathways were observed and they are illustrated in Scheme 1.

Different possible reaction pathways surmised on the basis of ESI–MS analyses. It is no doubt that hydroxyl radicals play a crucial role in the first step (hydroxylation of methylene blue) of dye degradation. As documented in [8], hydroxyl radicals are produced in the reaction between $HO_2^-$ species (formed in the interaction between $H_2O_2$ and hydroxyls from metal oxide surface) and $H_2O_2$ (Eq. (2)).

$$H_2O_{2(aq)} + HO_2^-{}_{(aq)} = HO\cdot_{(aq)} + O_2\cdot^-{}_{(aq)} + H_2O_{(aq)} \quad (2)$$

It was concluded that the role of $Nb_2O_5$ is to trap superoxo $O_2\cdot^-$ (and peroxo $O_2^{2-}$) species on the surface, leading to an increased production of the hydroxyl radicals ($O_2\cdot^-_{(aq)}$ + S-Nb(V)$_{(s)}$ = S-Nb(V)–$O_2\cdot^-_{(s)}$). Thus, the highest activity of $Nb_2O_5$ in the discoloration of methylene blue has to be related to hydroxyl radicals production. Similarly to $Nb_2O_5$, hydroxyl radicals were formed on the surface of $ZnNb_2O_6$ in reaction (Eq. (2)). Lower efficiency of methylene blue degradation observed for mixed niobium-zinc oxide in comparison to that of niobium pentoxide indicated that addition of zinc to niobium pentoxide and formation of mixed oxide reduced the $Nb_2O_5$ ability to trap of superoxo species. As the activity of mixed niobium-zinc oxide increased when the pH of reaction mixture was decreased, it was concluded that when $ZnNb_2O_6$ was used the concentration of $H^+$ must affect the HO· formation. Protons interact with superoxo radicals and therefore shift the reaction (Eq. (2)) equilibrium towards formation of hydroxyl radicals. It shows that the enhancement of $ZnNb_2O_6$ activity on decreasing pH of the reaction mixture resulted not only from enhanced adsorption of dye molecule, but mainly due to enhanced ability to hydroxyl radicals generation. Both for $Nb_2O_5$ and $ZnNb_2O_6$ the further and total oxidation rate of hydroxylated by-products of methylene blue degradation was determined by the oxygen species formed on the surface of metal oxides as followed from the ESI–MS spectra discussed below.

The discussion of ESI–MS spectra obtained within this work will be related to $m/z$ values assigned to different compounds presented in Scheme 1. Fig. 11 shows the ESI–MS spectra recorded for solutions after 1 h and 5 h of the reaction performed without pH adjustment. The signals at $m/z$ = 284 and 270 are attributed to methylene blue, and its demethylated form, respectively [12,54]. They are the only signals in MB mixed with water (Figs. 11A and B) and hydrogen peroxide (Figs. 11C and D), as well as in the mixture of ZnO with $H_2O_2$ (Figs. 11E and F). It is in a good agreement with earlier observation that ZnO was almost inactive in degradation of the dye. In the ESI–MS spectrum recorded for $ZnNb_2O_6$ after 1 h of the reaction a new signal at $m/z$ = 122 appeared (Fig. 11G). The relative intensity of this peak was small, that indicated a low conversion of the dye molecules. More significant changes in the ESI–MS spectrum were observed after 5 h of the reaction (Fig. 11H). The presence of new signals at $m/z$ = 300, 314, 332, 348 and 364 indicated consecutive additions of hydroxyls into the methylene blue. In addition to the peak at $m/z$ = 300 assigned to the hydroxylation of MB, another peak at $m/z$ = 303 was also observed. According to literature [55,56] this peak is attributed to formation of sulfoxide (see Scheme 1) by electronic reorganization during the transformation of MB adsorbed on the metal oxide surface. In this reaction path MB is chemisorbed via sulfur atom from MB on nucleophilic oxygen on the catalyst surface. Such chemisorption leads to the formation of sulfoxide which is further hydroxylated by hydroxyl radicals.

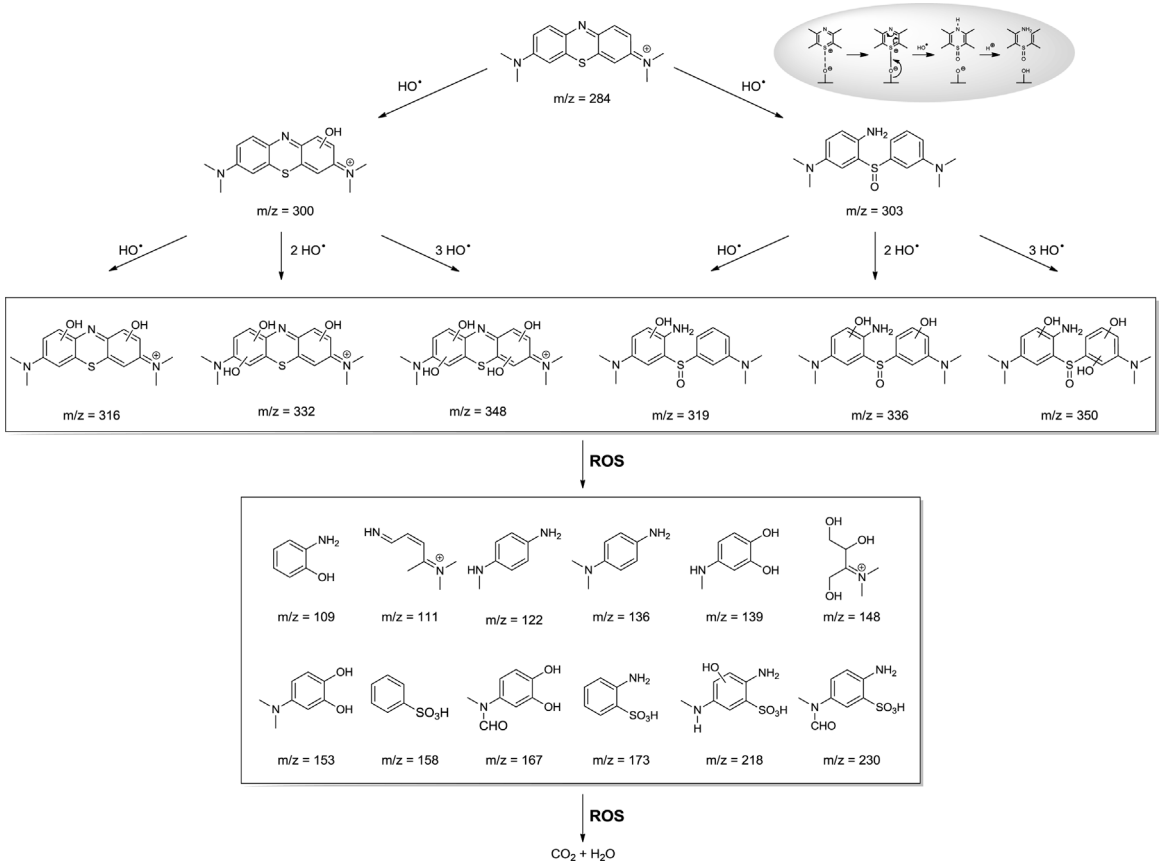


**Scheme 1.** Proposed pathways of methylene blue degradation with the use of $Nb_2O_5$ and $ZnNb_2O_6$ catalysts and $H_2O_2$ as oxidant (the identification of the compounds based on *m/z* values observed in ESI–MS spectra and came partially from literature data [11,12,14,50–56] and partially from calculations done within this work).

Surface oxygen is rebuilt by the interaction with hydroxyl radicals. The observation of a peak at $m/z = 303$ led to the conclusion that degradation of methylene blue proceeded via two different pathways. Since the intensity of the peak at $m/z = 300$ was much higher than that of the peak at $m/z = 303$, the pathway on which methylene blue molecule is directly hydroxylated appeared to be dominant. The presence of peaks at lower *m/z* ratio, i.e. 114, 122, 142, 150, 159 confirmed successful breaking up of the dye molecule into smaller fragments towards total degradation (see Scheme 1) [11,12,14,50–56] and indicated that discoloration of methylene blue solution in the reaction catalyzed by $ZnNb_2O_6$ proceeded via dye degradation.

ESI–MS analyses confirmed also very high activity of niobium pentoxide in the dye degradation process. For this metal oxide no methylene blue was observed even after 1 h of the reaction (UV-vis study revealed that this catalyst removed 97% of MB after 1 h of the reaction). It is important to stress that for the reaction with the use of $Nb_2O_5$ the peak at $m/z = 300$ characteristic of hydroxylated methylene blue molecule was definitely less intense than the signal at $m/z = 303$. Since the formation of sulfoxide took place at the surface of metal oxide, the higher surface area of niobium(V) oxide can be the reason of the higher capability of electronic reorganization of methylene blue molecule. High ability to sulfoxide formation may also result from a higher concentration of surface oxygen species on $Nb_2O_5$, than that estimated for ZnO and $ZnNb_2O_6$ (Table 3). Analysis of the products after 1 h of the reaction with the use of $Nb_2O_5$ revealed that the further steps of degradation process proceeded by consecutive hydroxylation of sulfoxide form (the peaks at $m/z = 303$, 319, 336, 350, 365 and 381). However, most of the fragmentation products that resulted from methylene blue ring rupture were similar to those observed for $ZnNb_2O_6$ as a catalyst (peaks at $m/z = 121$, 139, 158, 175). Fig. 11I and J clearly show that with increasing reaction time the relative intensity of the peaks characteristic of degradation products was significantly reduced (especially for the products of methylene blue ring rupture, i.e. peaks at $m/z < 200$), that indicated their total degradation (oxidation). After 5 h of the reaction the most intense peaks were observed at $m/z = 319$ and 336. This indicated relatively high stability of hydroxylated sulfoxide. ESI–MS analyses were also performed for the reactions with higher concentration of MB solution (37.5 mg $L^{-1}$; Fig. 11K). It was found that besides the peak characteristic of sulfoxide (Fig. 11K; $m/z = 303$), the peak typical of hydroxylated methylene blue was also observed ($m/z = 300$). It is worth of notice that at higher dye concentration the relative intensity of the peak at $m/z = 300$ was also lower than that of the peak at $m/z = 303$. Since after 5 h of the reaction the peak at $m/z = 300$ was not observed (Fig. 11L), and the peak at $m/z = 303$ was still present, it was concluded that the species characterized by the former peak is more liable to oxidation. Faster degradation of methylene blue through formation of the compound characterized by $m/z = 300$ was also concluded from the significant decrease in intensity of the peaks at $m/z = 317$, 331 and 348. Similarly to the reaction with the lower concentration of the dye, after 5 h of oxidation process the most intense peaks in ESI–MS spectrum were observed at $m/z = 303$, 319, 336 (products of sulfoxide hydroxylation).

The above discussed results indicated for the first time that in the presence of both oxides ($Nb_2O_5$ and $ZnNb_2O_6$) the reaction of methylene blue discoloration occurred via two different paths in parallel. Both involved hydroxyl radicals in the first step of the reaction. In one reaction pathway the direct hydroxylation of MB occurred, whereas in the other MB was chemisorbed on nucleophilic surface oxygen, next oxidized by this oxygen to sulfoxide and sulfoxide was then hydroxylated by hydroxyl radicals. The relative participation of both reaction pathways in the methylene blue degradation depended on the competition between chemisorption of MB and direct hydroxylation. The ability of

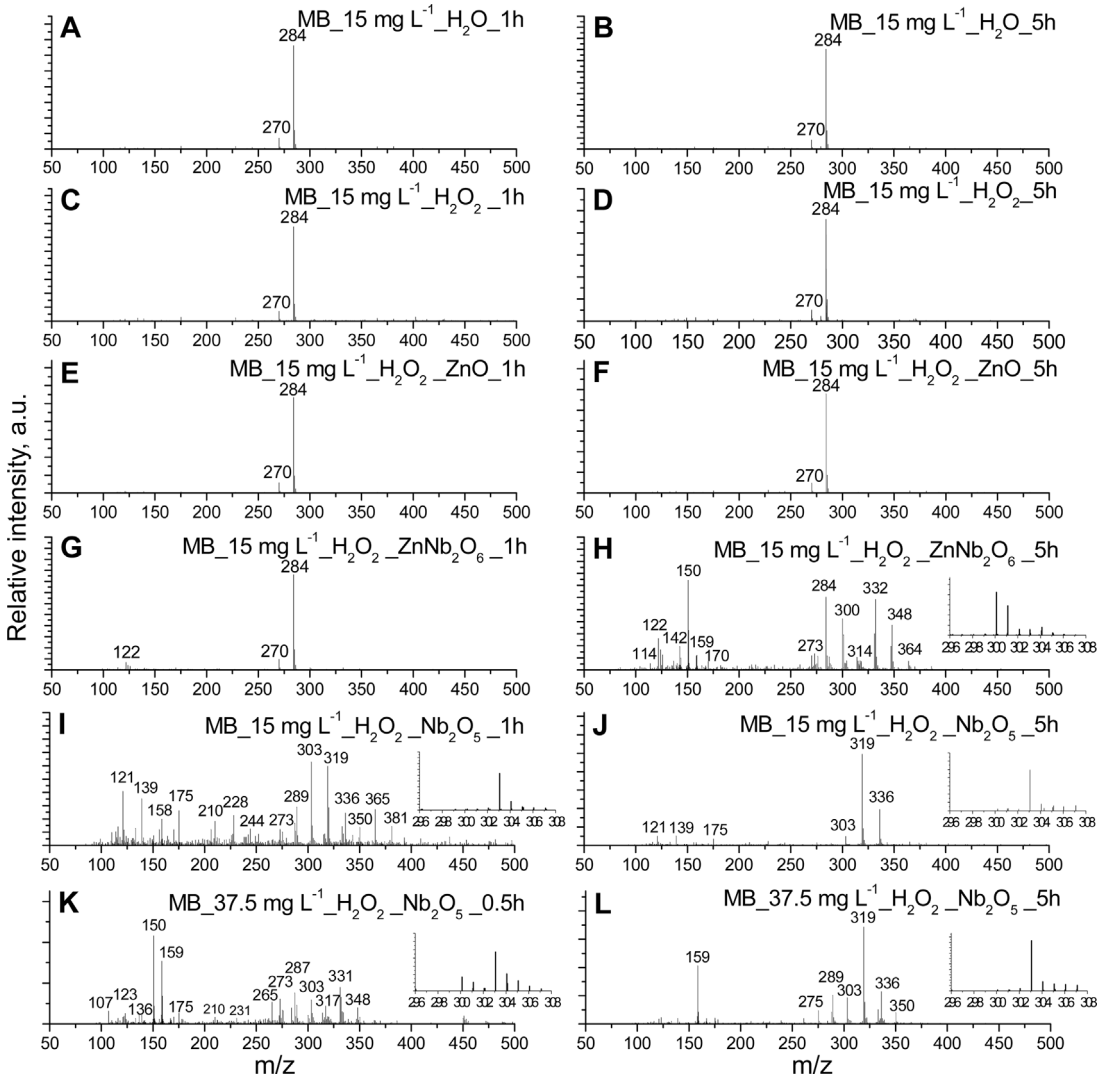


**Fig. 11.** ESI mass spectra of methylene blue solutions after 1 h and 5 h of the reaction.

MB to be chemisorbed, as well as the efficiency of the production of hydroxyl radicals were determined by the surface properties of the solids, different for all oxides used in this work. The hydroxylation process was faster on niobium(V) oxide than on mixed niobium-zinc oxide as concluded from the appearance of the hydroxylation products already after 1 h of the reaction in the presence/over the first material. Niobium(V) oxide exhibited higher surface area and high ability in the formation of hydroxyl radicals [8]. The following reaction steps, decomposition of the hydroxylated intermediates and finally total oxidation occurred with the participation of reactive oxygen species (ROS) formed on the surface of the solids after interaction with hydrogen peroxide. Niobium pentoxide and mixed niobium-zinc oxide exhibited different surface properties. This affected the type of reactive oxygen species formed on the surface of metal oxides. $Nb_2O_5$ treatment with hydrogen peroxide led to the formation of peroxo and superoxo surface species, while in the presence of $ZnNb_2O_6$ only superoxo and hydrogen-superoxo species were identified. Peroxo species are known to be very active in terms of interaction with C=C bonds, and thus they may facilitate the degradation of dye molecule. Oliveira et al. [52] have shown that $O_2^{2-}$ species formed on the surface of vanadium-doped iron oxide were highly active in degradation of methylene blue. This permitted us to conclude that the higher activity of niobium pentoxide in the degradation of hydroxylated intermediates was caused also by the formation of peroxo species on its surface, and that peroxo species were much more active in degradation of methylene blue than superoxo species.

The lowest activity in methylene blue degradation process was characteristic of ZnO. FTIR, UV–vis and XPS studies revealed that the interaction of this metal oxide with hydrogen peroxide led to the formation of both peroxo and superoxo species. Thus, this material was supposed to be active in methylene blue degradation. In contrast to $ZnNb_2O_6$ and $Nb_2O_5$, zinc oxide exhibited very low surface area. However, not the low surface area was responsible for the lack of ZnO activity because in the experiment with the use of commercial zinc oxide (ZnO, US Research Nanomaterials Inc., surface area: 40–70 $m^2\,g^{-1}$; pH of reaction mixture: 6.5, MB concentration: 37.5 mg $L^{-1}$) after 3 h of the reaction no significant MB conversion was observed. The probable reason for the low activity of ZnO in methylene blue degradation was the formation of $ZnO_2$. Analysis of surface composition of ZnO after treatment with $H_2O_2$ by XPS indicated a significant increase in the concentration of surface oxygen species (increase from 47.9 at% for ZnO to 56.5 at% – Table 3) which was caused by $ZnO_2$ formation. It was found that the concentration of peroxo species was several times higher than on the other oxides used in this work that most probably limited the generation of hydroxyl radicals necessary in the first step of the reaction. This issue will be the subject of a separate paper.

## 4. Conclusions

In this work we have synthesized $Nb_2O_5$, ZnO and $ZnNb_2O_6$ by the use of solvent evaporation method and characterized the structure and surface properties of the obtained oxides also after interaction with hydrogen peroxide used in the degradation of methylene blue. The obtained results indicated that the formation of cation-deficient species containing highly nucleophilic oxygen as a result of the interaction of metal oxides with hydrogen peroxide was easier on the surface of $ZnNb_2O_6$ than on $Nb_2O_5$. It was also proved that the interaction of metal oxides used in this work with hydrogen peroxide generated also superoxo species on all samples, and additionally peroxo species on the surface of $Nb_2O_5$ and ZnO. It was found that the formation of peroxo species on the surface of $Nb_2O_5$ was related to the presence of Nb═O bonds, and was strongly affected by the length of these bonds. The shortening of Nb═O bond length, which was characteristic of $ZnNb_2O_6$, prevented the formation of surface peroxo species.

Niobium(V) oxide was the most effective catalyst in methylene blue degradation with hydrogen peroxide. MB degradation process occurred via two parallel reaction pathways: i) direct hydroxylation of MB with hydroxyl radicals and ii) hydroxylation (by HO· radicals) of MB sulfoxide formed by chemisorption of MB and oxidation with surface oxygen rebuilt with HO· radicals. Both paths were identified on niobium pentoxide and mixed niobium-zinc oxide. In the following degradation of MB hydroxylated intermediates surface peroxo species played a crucial role. The formation of $ZnO_2$ in the interaction with $H_2O_2$ was supposed to limit hydroxyl radicals formation and to be responsible for the lack of ZnO activity in MB degradation.

## Acknowledgements

This work was supported by the National Science Centre in Poland (Grants No. 2016/21/N/ST5/00533 and 2013/10/E/ST5/00642), and the European Union (Project No.UDA-POKL.04.01.01-00-109/13). Lukasz Wolski wishes to thank Prof. James Whitten from the UMass Lowell for training in SEM and SEM-EDX measurements and for permission for performance of measurements needed for this study at the University of Massachusetts Lowell, Dr. Izabela Sobczak and Dr. Anna Wojtaszek-Gurdak from Adam Mickiewicz University in Poznan for the investigation of hydroxyl radicals generation with the use of OPD substrate and very helpful discussion.

## Appendix A. Supplementary data

Supplementary data associated with this article can be found, in the online version, at http://dx.doi.org/10.1016/j.apcatb.2017.11.008.

## References

[1] I.W.C.E. Arends, R.A. Sheldon, Modern oxidation of alcohols using environmentally benign oxidants, Mod. Oxid. Methods, Wiley-VCH Verlag GmbH & Co. KGaA, FRG, Weinheim, 2005, pp. 83–118, http://dx.doi.org/10.1002/3527603689.ch4.
[2] N.E. Thornburg, S.L. Nauert, A.B. Thompson, J.M. Notestein, Synthesis-structure-function relationships of silica-supported niobium(V) catalysts for alkene epoxidation with $H_2O_2$, ACS Catal. 6 (2016) 6124–6134, http://dx.doi.org/10.1021/acscatal.6b01796.
[3] L.C. Passoni, M.R.H. Siddiqui, A. Steiner, I.V. Kozhevnikov, Niobium peroxo compounds as catalysts for liquid-phase oxidation with hydrogen peroxide, J. Mol. Catal. A Chem. 153 (2000) 103–108, http://dx.doi.org/10.1016/S1381-1169(99)00307-6.
[4] S. Verma, S.L. Jain, Nanosized zinc peroxide ($ZnO_2$): a novel inorganic oxidant for the oxidation of aromatic alcohols to carbonyl compounds, Inorg. Chem. Front. 1 (2014) 534–539, http://dx.doi.org/10.1039/C3QI00092C.
[5] O.A. Kholdeeva, Recent developments in liquid-phase selective oxidation using environmentally benign oxidants and mesoporous metal silicates, Catal. Sci. Technol. 4 (2014) 1869–1889, http://dx.doi.org/10.1039/c4cy00087k.
[6] M. Ziolek, P. Decyk, I. Sobczak, M. Trejda, J. Florek, H. Golinska, W. Klimas, A. Wojtaszek, Catalytic performance of niobium species in crystalline and amorphous solids–gas and liquid phase oxidation, Appl. Catal. A Gen. 391 (2011) 194–204, http://dx.doi.org/10.1016/j.apcata.2010.07.022.
[7] M. Ziolek, I. Sobczak, P. Decyk, L. Wolski, The ability of $Nb_2O_5$ and $Ta_2O_5$ to generate active oxygen in contact with hydrogen peroxide, Catal. Commun. 37 (2013) 85–91, http://dx.doi.org/10.1016/j.catcom.2013.03.032.
[8] M. Ziolek, I. Sobczak, P. Decyk, K. Sobańska, P. Pietrzyk, Z. Sojka, Search for reactive intermediates in catalytic oxidation with hydrogen peroxide over amorphous niobium(V) and tantalum(V) oxides, Appl. Catal. B Environ. 164 (2015) 288–296, http://dx.doi.org/10.1016/j.apcatb.2014.09.024.
[9] M. Ziolek, I. Sobczak, The role of niobium component in heterogeneous catalysts, Catal. Today 285 (2017) 211–225, http://dx.doi.org/10.1016/j.cattod.2016.12.013.
[10] H. Shima, M. Tanaka, H. Imai, T. Yokoi, T. Tatsumi, J.N. Kondo, IR observation of selective oxidation of cyclohexene with $H_2O_2$ over mesoporous $Nb_2O_5$, J. Phys. Chem. C. 113 (2009) 21693–21699, http://dx.doi.org/10.1021/cm100391q.
[11] K. Dutta, S. Mukhopadhyay, S. Bhattacharjee, B. Chaudhuri, Chemical oxidation of methylene blue using a Fenton-like reaction, J. Hazard. Mater. 84 (2001) 57–71, http://dx.doi.org/10.1016/S0304-3894(01)00202-3.
[12] D. Wiedmer, E. Sagstuen, K. Welch, H.J. Haugen, H. Tiainen, Oxidative power of aqueous non-irradiated $TiO_2$-$H_2O_2$ suspensions: methylene blue degradation and the role of reactive oxygen species, Appl. Catal. B: Environ. 198 (2016) 9–15, http://dx.doi.org/10.1016/j.apcatb.2016.05.036.
[13] A. Esteves, L.C.A. Oliveira, T.C. Ramalho, M. Goncalves, A.S. Anastacio, H.W.P. Carvalho, New materials based on modified synthetic $Nb_2O_5$ as photocatalyst for oxidation of organic contaminants, Catal. Commun. 10 (2008) 330–332, http://dx.doi.org/10.1016/j.catcom.2008.09.012.
[14] L.C.A. Oliveira, M. Gonçalves, M.C. Guerreiro, T.C. Ramalho, J.D. Fabris, M.C. Pereira, K. Sapag, A new catalyst material based on niobia/iron oxide composite on the oxidation of organic contaminants in water via heterogeneous Fenton mechanisms, Appl. Catal. A Gen. 316 (2007) 117–124, http://dx.doi.org/10.1016/j.apcata.2006.09.027.
[15] F.P. Cardoso, A.E. Nogueira, P.S.O. Patrício, L.C.A. Oliveira, Effect of tungsten doping on catalytic properties of niobium oxide, J. Braz. Chem. Soc. 23 (2012) 702–709.
[16] H.-J. Lee, K.-S. Hong, S.-J. Kim, I.-T. Kim, Dielectric properties of $MNb_2O_6$ compounds (where M = Ca, Mn, Co, Ni, OR Zn), Mater. Res. Bull. 32 (1997) 847–855, http://dx.doi.org/10.1016/S0025-5408(97)00034-2.
[17] M. Maeda, T. Yamamura, T. Ikeda, Dielectric characteristics of several complex oxide ceramics at microwave frequencies, Jpn. J. Appl. Phys. 26 (1987) 76–79.
[18] H.B. Bafrooei, E.T. Nassaj, C.F. Hu, Q. Huang, T. Ebadzadeh, Microwave sintering of nanopowder $ZnNb_2O_6$: Densification, microstructure and microwave dielectric properties, Phys. B: Condens. Matter. 454 (2014) 35–41, http://dx.doi.org/10.1016/j.physb.2014.07.024.
[19] W. Wu, S. Liang, Z. Ding, H. Zheng, L. Wu, A new approach to the preparation of microcrystalline $ZnNb_2O_6$ photocatalysts via a water-soluble niobium-citrate-peroxo compound, Solid State Sci. 13 (2011) 2019–2023, http://dx.doi.org/10.1016/j.solidstatesciences.2011.08.032.
[20] W. Wu, S. Liang, Z. Ding, H. Zheng, L. Wu, Low temperature synthesis of nanosized $ZnNb_2O_6$ photocatalysts by a citrate complex method, J. Sol-Gel Sci. Technol. 61 (2012) 570–576, http://dx.doi.org/10.1007/s10971-011-2661-y.
[21] A. Kudo, S. Nakagawa, H. Kato, Overall water splitting into $H_2$ and $O_2$ under UV irradiation on NiO-loaded $ZnNb_2O_6$ photocatalysts consisting of $d^{10}$ and $d^0$ ions, Chem. Lett. 28 (1999) 1197–1198, http://dx.doi.org/10.1246/cl.1999.1197.
[22] N. Suzuki, T. Athar, Y. Huang, K. Shimasaki, N. Miyamoto, Y. Yamauchi, Synthesis of mesoporous $Nb_2O_5$ with crystalline walls and investigation of their photocatalytic activity, J. Ceram. Soc. Japan 6 (2011) 405–411.
[23] J. Tauc, R. Grigorovici, A. Vancu, Optical properties and electronic structure of amorphous germanium, Phys. Stat. Sol. 15 (1966) 627–637, http://dx.doi.org/10.1016/0025-5408(68)90023-8.
[24] K. Sobanska, P. Pietrzyk, Z. Sojka, Generation of reactive oxygen species via electroprotic interaction of $H_2O_2$ with $ZrO_2$ gel: ionic sponge effect and pH-switchable peroxidase- and catalase-like activity, ACS Catal. 7 (2017) 2935–2947, http://dx.doi.org/10.1021/acscatal.7b00189.
[25] P. Yang, D. Zhao, D.I. Margolese, B.F. Chmelka, G.D. Stucky, Block copolymer templating syntheses of mesoporous metal oxides with large ordering lengths and semicrystalline framework, Chem. Mater. 11 (1999) 2813–2826, http://dx.doi.org/10.1021/cm990185c.
[26] G. Belous, O.V. Ovchar, V. Kramarenko, B. Jancar, J. Bezjak, D. Suvorov, Synthesis and microwave dielectric properties of $Zn_{1+x}Nb_2O_{6+x}$, Inorg. Mater. 43 (2007) 277–280, http://dx.doi.org/10.1134/S0020168507030120.
[27] R.C. Pullar, The synthesis, properties, and applications of columbite niobates ($M^{2+}Nb_2O_6$): A critical review, J. Am. Ceram. Soc. 92 (2009) 563–577, http://dx.doi.org/10.1111/j.1551-2916.2008.02919.x.
[28] F. García-Alvarado, A. Orera, J. Canales-Vázquez, J.T.S. Irvine, On the electrical properties of synthetic manganocolumbite $MnNb_2O_{6-\delta}$, Chem. Mater. 18 (2006) 3827–3834, http://dx.doi.org/10.1021/cm0603203.
[29] J.-M. Jehng, I.E. Wachs, Molecular structures of supported niobium oxide catalysts under in situ conditions, J. Phys. Chem. 95 (1991) 7373–7379.
[30] L.J. Burcham, J. Datka, I.E. Wachs, In situ vibrational spectroscopy studies of supported niobium oxide catalysts, J. Phys. Chem. B 103 (1999) 6015–6024, http://dx.doi.org/10.1021/jp990289a.
[31] D.C. Castro, R.P. Cavalcante, J. Jorge, M.A.U. Martines, L.C.S. Oliveira, G.A. Casagrande, A. Machulek Jr., Synthesis and characterization of mesoporous $Nb_2O_5$ and its application for photocatalytic degradation of the herbicide methyl-viologen, J. Braz. Chem. Soc. 27 (2016) 303–313.
[32] Y. Zheng, C. Chen, Y. Zhan, X. Lin, Q. Zheng, K. Wei, J. Zhu, Y. Zhu, Luminescence and photocatalytic activity of ZnO nanocrystals: correlation between structure and property, Inorg. Chem. 46 (2007) 6675–6682, http://dx.doi.org/10.1021/ic062394m.

[33] A.G.S. Prado, L.B. Bolzon, C.P. Pedroso, A.O. Moura, L.L. Costa, $Nb_2O_5$ as efficient and recyclable photocatalyst for indigo carmine degradation, Appl. Catal. B: Environ. 82 (2008) 219–224, http://dx.doi.org/10.1016/j.apcatb.2008.01.024.
[34] S.M. Lam, J.C. Sin, I. Satoshi, A.Z. Abdullah, A.R. Mohamed, Enhanced sunlight photocatalytic performance over $Nb_2O_5$/ZnO nanorod composites and the mechanism study, Appl. Catal. A Gen. 471 (2014) 126–135, http://dx.doi.org/10.1016/j.apcata.2013.12.001.
[35] L. Wolski, J.E. Whitten, I. Sobczak, M. Ziolek, The effect of the preparation procedure on the morphology, texture and photocatalytic properties of ZnO, Mater. Res. Bull. 85 (2016) 35–46, http://dx.doi.org/10.1016/j.materresbull.2016.08.027.
[36] M. Strongin, S.L. Qiu, J. Chen, C.L. Lin, E.M. McCarron, Question of superoxide in $La_2CuO_{4+\delta}$, Phys. Rev. B. 41 (1990) 7238–7240, http://dx.doi.org/10.1103/PhysRevB.41.7238.
[37] K. Kim, J.-R. Cha, M.-S. Gong, J.-G. Kim, Preparation of $ZnO_2$ nanoparticles using organometallic zinc(II) isobutylcarbamate in organic solvent, Bull. Korean Chem. Soc. 35 (2014) 431–435, http://dx.doi.org/10.5012/bkcs.2014.35.2.431.
[38] D. Srinivas, P. Manikandan, S.C. Laha, R. Kumar, P. Ratnasamy, Reactive oxo-titanium species in titanosilicate molecular sieves: EPR investigations and structure-activity correlations, J. Catal. 217 (2003) 160–171, http://dx.doi.org/10.1016/S0021-9517(03)00060-5.
[39] L. Moreno-Real, E.R. Losilla, M.A.G. Aranda, M. Martínez-Lara, S. Bruque, M. Gabás, A peroxoniobium phosphate derived from $NbOPO_4.3H_2O$, J. Solid State Chem. 137 (1998) 289–294, http://dx.doi.org/10.1006/jssc.1997.7738.
[40] L. Spanhel, M.A. Anderson, Semiconductor clusters in the sol-gel process: quantized aggregation, gelation, and crystal growth in concentrated ZnO colloids, J. Am. Chem. Soc. 113 (1991) 2826–2833, http://dx.doi.org/10.1021/ja00008a004.
[41] T.A. Saleh, M.A. Gondal, Q.A. Drmosh, Z.H. Yamani, A. AL-yamani, Enhancement in photocatalytic activity for acetaldehyde removal by embedding ZnO nano particles on multiwall carbon nanotubes, Chem. Eng. J. 166 (2011) 407–412, http://dx.doi.org/10.1016/j.cej.2010.10.070.
[42] Z. Chen, Q. Gao, M. Ruan, J. Shi, Zinc oxide nanoarrays in nanoporous nickel phosphate with a huge blueshift ultraviolet-visible exciton absorption peak, Appl. Phys. Lett. 87 (2005) 93113, http://dx.doi.org/10.1063/1.2035318.
[43] H. Bai, X. Liu, Green hydrothermal synthesis and photoluminescence property of $ZnO_2$ nanoparticles, Mater. Lett. 64 (2010) 341–343, http://dx.doi.org/10.1016/j.matlet.2009.11.008.
[44] M. Che, A.J. Tench, Characterization and reactivity of molecular oxygen species on oxide surfaces, Adv. Catal. 32 (1983) 1–148, http://dx.doi.org/10.1016/S0360-0564(08)60439-3.
[45] S. Nayak, P.U. Biedermann, M. Stratmann, A. Erbe, A mechanistic study of the electrochemical oxygen reduction on the model semiconductor n-Ge(100) by ATR-IR and DFT, Phys. Chem. Chem. Phys. 15 (2013) 5771–5781, http://dx.doi.org/10.1039/c2cp43909c.
[46] J. Sala-Pala, J. Roue, J.E. Guerchais, Study of a new type of transition metal peroxo complexes as oxidants, J. Mol. Catal. 7 (1980) 141–148.
[47] N.T. Prado, F.G.E. Nogueria, A.E. Nogueira, C.A. Nunes, R. Diniz, L.C.A. Oliveira, Modified niobia as a new catalyst for selective production of dimethoxymethane from methanol, Energy Fuels 24 (2010) 4793–4796, http://dx.doi.org/10.1021/ef100876k.
[48] A.A. Hoffmann, S.L.P. Dias, J.R. Rodrigues, F.A. Pavan, E.V. Benvenutti, E.C. Lima, Methylene blue immobilized on cellulose acetate with titanium dioxide: an application as sensor for ascorbic acid, J. Braz. Chem. Soc. 19 (2008) 943–949, http://dx.doi.org/10.1590/S0103-50532008000500020.
[49] S. Sohrabnezhad, A. Pourahmad, R. Rakhshaee, A. Radaee, S. Heidarian, Catalytic reduction of methylene blue by sulfide ions in the presence of nanoAlMCM-41 material, Superlattices Microstruct. 47 (2010) 411–421, http://dx.doi.org/10.1016/j.spmi.2009.12.006.
[50] A. Molla, M. Sahu, S. Hussain, Under dark and visible light: fast degradation of methylene blue in the presence of Ag–In–Ni–S nanocomposites, J. Mater. Chem. A. 3 (2015) 15616–15625, http://dx.doi.org/10.1039/C5TA02888D.
[51] H.-P. Jing, C.-C. Wang, Y.-W. Zhang, P. Wang, R. Li, Photocatalytic degradation of methylene blue in ZIF-8, RSC Adv. 4 (2014) 54454–54462, http://dx.doi.org/10.1039/C4RA08820D.
[52] H.S. Oliveira, L.C.A. Oliveira, M.C. Pereira, J.D. Ardisson, P.P. Souza, P.O. Patrício, F.C.C. Moura, Nanostructured vanadium-doped iron oxide: catalytic oxidation of methylene blue dye, New J. Chem. 39 (2015) 3051–3058, http://dx.doi.org/10.1039/C4NJ02063D.
[53] M.A. Rauf, M.A. Meetani, A. Khaleel, A. Ahmed, Photocatalytic degradation of Methylene Blue using a mixed catalyst and product analysis by LC/MS, Chem. Eng. J. 157 (2010) 373–378, http://dx.doi.org/10.1016/j.cej.2009.11.017.
[54] H.W.P. Carvalho, A.P.L. Batista, P. Hammer, T.C. Ramalho, Photocatalytic degradation of methylene blue by $TiO_2$-Cu thin films: theoretical and experimental study, J. Hazard. Mater. 184 (2010) 273–280, http://dx.doi.org/10.1016/j.jhazmat.2010.08.033.
[55] S. Xia, L. Zhang, G. Pan, P. Qian, Z. Ni, Photocatalytic degradation of methylene blue with a nanocomposite system: synthesis, photocatalysis and degradation pathways, Phys. Chem. Chem. Phys. 17 (2015) 5345–5351, http://dx.doi.org/10.1039/C4CP03877K.
[56] A. Houas, H. Lachheb, M. Ksibi, E. Elaloui, C. Guillard, J.M. Herrmann, Photocatalytic degradation pathway of methylene blue in water, Appl. Catal. B: Environ. 31 (2001) 145–157, http://dx.doi.org/10.1016/S0926-3373(00)00276-9.